

**Ionization Cross Sections of Silane and Disilane by  
Electron impact**

B. Krishnakumar\* and S. K. Srivastava

*Jet Propulsion laboratory, California Institute of Technology*

*46'00 Oak Grow Drive, Pasadena, CA 91109, U.S.A.*

**Abstract**

Partial ionization cross sections for silane and disilane by electron impact have been measured for electron energies in the range of threshold to 1000 eV using a crossed beam geometry and employing a pulsed electron beam and a pulsed ion extraction technique. The cross sections were normalized by using the relative flow technique. For ease of use in various plasma modeling we have fitted the cross sections to an empirical formulae.

## 1. INTRODUCTION

Ionization of molecules produces various fragment ions with yields depending on the energy of the ionizing agent and the nature of the molecule. This process, called dissociative ionization, is a major contributing factor to the gross ionization cross section in the case of molecules. Most of these fragment ions generally have substantial amount of kinetic energies and, therefore, special care is needed for making accurate measurements of the cross sections. This is particularly true for electron impact dissociative ionization of molecules where special efforts have to be made to extract ions formed in the interaction region without affecting the electron beam. As a result, relatively few measurements have been reported on these molecules. Recently, we have used a pulsed electron beam in combination with a pulsed ion extraction technique to ensure complete collection of all ions irrespective of their initial kinetic energies without affecting the electron beam [1]. Here, we report our measurements on silane and disilane using the same technique. Normalized values of cross sections have been obtained by using the relative flow technique [1,2].

Silane and disilane are very important molecules for the semiconductor industry. Cross sections for the formation of various ions by electron impact ionization of these molecules are essential in modeling the plasmas containing these molecules. Even though several reports have been published in the past on the appearance energies of various positive fragment ions from silanes [3,7], there is only one on the measurement of absolute cross sections as a function of incident electron energy for these molecules. This is by Chatham *et al.* [8] in the energy range from threshold to 200 eV for both silane and disilane. Turban *et al.* [9] have reported the relative values of cross sections in the range of 10 to 90 eV for silane. This measurement is more of historical value as the

apparatus and the operating conditions used by Turban *et al.* [9] were not really designed for studying the variation of cross sections as a function of electron impact energy. Chatham *et al.* made three different experiments to obtain the absolute values of cross sections as a function of electron impact energy. In their first set up the total ionization cross section for each gas was measured relative to that of an inert gas whose ionization cross section was well known. This measurement was free of ion mass and kinetic energy discriminate ion effects. In the second set up they obtained cracking patterns (i.e., spectra of fragment ions) by minimizing the discrimination effects, but at the cost of electron energy resolution. In the third set up they optimized the energy resolution and obtained the relative cross sections as a function of the electron impact energy. These were then normalized to obtain absolute partial cross sections using the data from the first two experimental set ups. We routinely use the relative flow technique [1,2] for these types of measurements which provides normalized values of cross sections with one experimental set up. In the following, the procedure for measuring these cross sections and their values are presented and compared with previous data.

## II. EXPERIMENTAL DETAILS

A schematic diagram of the apparatus used for the present measurements is shown in Fig. 1. Detailed description of the apparatus and experimental procedure has been published earlier [1,2]. A brief description is as follows. A magnetically collimated and pulsed electron beam is crossed at right angles with a thermal molecular beam formed by a capillary array. The electron beam is monitored by a Faraday cup. Ions formed in the interaction region are extracted by an electric field

applied between two molybdenum wire meshes placed symmetrical 1 y on either side of the interaction region. The ions are then focussed at the entrance aperture of a quadrupole mass spectrometer by a set of electrostatic lenses. The mass selected ions are detected by a channel electron multiplier operated in the pulse counting mode. The ion extraction field is applied in a pulsed form in such a way that when the electron beam is present in the interaction region it is at ground potential. This arrangement enables us to apply sufficiently high fields to collect all ions with initial kinetic energies as high as 5 eV, without affecting the electron beam.

Pure silane and disilane were obtained from Matheson and special efforts were made to avoid contamination with moisture and air. In a first step, excitation functions for each fragment ion were obtained as a function of electron impact energy. Measurements were carried out with a base pressure of about  $1 \times 10^{-7}$  Torr and a time averaged electron beam current of 1 nA. Relative values of cross sections, thus obtained, were subsequently normalized using the relative flow technique. For this purpose the overall detection efficiency, which is the combined efficiency of transmission of the quadrupole mass analyzer and the detection efficiency of the channeltron, was determined using the rare gas ionization procedure discussed in our previous publications [1,2]. For determining the absolute values of cross sections for various fragment ions we had to make additional corrections for the isotopic concentrations of Si. Si has three isotopes of masses 28, 29, and 30 with abundances of 92.23%, 4.67% and 3.10%, respectively. We estimate that the uncertainty in the values of relative cross sections in the present measurements is about 10% and that in the absolute values of cross sections it is 15%.

## 11. RESULTS AND DISCUSSIONS

### A. Silane

Present results are shown in Figure 2. Also shown are the data reported by Chatham *et al.* [8]. Table 1 provides numerical values of cross sections. As reported by Chatham *et al.*, we find that ions formed from the dissociative ionization of  $\text{SiH}_4$  are  $\text{SiH}_3^+$ ,  $\text{SiH}_2^+$ ,  $\text{SiH}^+$ ,  $\text{Si}^+$ ,  $\text{H}_2^+$  and  $\text{H}^+$ . No  $\text{SiH}_4^+$  is observed. The absence of  $\text{SiH}_4^+$  has been established earlier by Potzinger and Lampe [7] and Morrison and Traeger [3]. It is due to the predissociation of  $\text{SiH}_4$  into  $\text{SiH}_3$  and  $\text{H}_2$  and has been corroborated by the enhanced intensity of  $\text{SiH}_2^+$  as compared to that of  $\text{SiH}_3^+$ , giving support to this explanation. However, our measurements show substantial deviations from the results reported by Chatham *et al.* in this regard. We observe maximum value of the  $\text{SiH}_3^+$  cross section at about 30 eV electron impact energy whereas Chatham *et al.* find this around 45 eV. Also both the relative shape and absolute cross sections in the 30 to 200 eV range show appreciable differences. For  $\text{SiH}_3^+$  there is less divergence in the relative shape even though we see a shallow dip in the cross section centered at about 38 eV electron impact energy. However, the absolute value of the cross section differs by about 40%. The relative shape and magnitude of the cross sections of  $\text{SiH}_2^+$  are in good agreement up to 50 eV, beyond which the data of Chatham *et al.* seem to fall much too slowly, with the cross sections at 200 eV differing by a factor of two. The cross sections for the formation of  $\text{Si}^+$  are in good agreement in the two measurements. The  $\text{H}_2^+$  cross section in our data peaks at about 65 eV whereas Chatham *et al.* obtain the peak at approximately 100 eV and the absolute value of the cross section at 200 eV is a factor of two larger than that we measure at that energy. The biggest difference in the two measurements seem to be in the absolute magnitude of the  $\text{H}^+$  data, the present being a factor of seven smaller at 100 eV.

From a qualitative point of view, it is interesting to note the nature of the  $\text{H}^+$  cross sections, as compared to the cross sections for the formation of other ions. In the present experiment, as well as that of Chatham *et al.*, the peak of  $\text{H}^+$  cross sections is substantially shifted to the high energy side.

The appearance potentials for positive ions from  $\text{SiH}_4$  are given in Table 11. The large uncertainty in  $\text{H}^+$  and  $\text{H}_2^+$  is due to the difficulty in eliminating the background counts from  $\text{H}_2\text{O}$  and other hydrocarbons present in the background. There seems to be good agreement on the appearance potential of silicon ion and its hydride ions. None of the earlier reports, except by Neuert and Clasen [4], have given the appearance potentials for  $\text{H}^+$  and  $\text{H}_2^+$ . Our value of  $\text{H}_2^+$  threshold is considerably different from that of Neuert and Clasen.

## B. Disilane

The cross sections for the formation of various positive ions from disilane are shown in Fig. 3 and presented in Table 11. In Fig. 3 we also include cross sections obtained by Chatham *et al.* [8]. Our data are quite different from theirs in both relative shape and magnitude. The exceptions to this are data for  $\text{Si}_2\text{H}_6^+$  and  $\text{Si}_2\text{H}_5^+$  where both relative shape and absolute magnitudes are in good agreement. In the case of  $\text{Si}_2\text{H}_4^+$  also there seems to be a fair agreement in the data, though we see a double hump with peaks at about 30 and 60 eV, respectively, as opposed to a structureless shape peaking at about 60 eV [8]. In the case of  $\text{Si}_2\text{H}_3^+$  we see a peak at 27 eV which is different from the broad structure with a peak at about 100 eV observed by Chatham *et al.* Our results on  $\text{Si}_2\text{H}_2^+$  and  $\text{Si}_2\text{H}^+$  also show a double hump with the first peak being very prominent at about 30 and 32 eV, respectively. The data of Chatham *et al.* also show this double peaked structure for these two ions. However, there are substantial differences in the relative shape and absolute values of cross sections.

## REFERENCES

\* Present address: Tata institute of Fundamental Research, Bombay 400005, India.

- [1] E. Krishnakumar and S. K. Srivastava, *J. Phys. B: At. Mol. Opt. Phys.* 21, 1055 (1988).
- [2] E. Krishnakumar and S. K. Srivastava, *J. Phys. B: At. Mol. Opt. Phys.* 23, 1893 (1991).
- [3] J. P. Morrison and J. C. Traeger, *Int. J. Mass Spectrom. Ion Phys.* 11, 289 (1973).
- [4] H. Neuret and I. Clasen, *Z. Naturforsch.* 7a, 41 (1952).
- [5] W. C. Steele, L. D. Nichols and F. A. Stone, *J. Amer. Chem. Soc.* 84, 4441 (1962).
- [6] F. E. Saalfeld and H. J. Svec, *Inorg. Chem.* 2, 46 (1963).
- [7] P. Potzinger and F. W. Lampe, *J. Phys. Chem.* 73, 3912 (1969).
- [8] H. Chatham, D. Hills, R. Robertson and A. Gallagher, *J. Chem. Phys.* 81, 1770 (1984).
- [9] G. Turban, Y. Catherine and B. Grolleau, *Thin Solid Films* 67, 309 (1980).
- [10] K. L. Bell, I. I. Gilbody, J. G. Hughs, A. E. Kingston, and F. J. Smith, *J. Chem. Ref. Data* 12, 891 (1983).
- [11] S. K. Srivastava and H. P. Nguyen, *JPL Report #87-2* (1987).

TABLE I. Partial and total ionization cross sections ( $10^{-18} \text{ cm}^2$ ) of  $\text{SiH}_4$

Electron	$\text{H}^+$	$\text{H}_2^+$	$\text{Si}^+$	$\text{SiH}^+$	$\text{SiH}_2^+$	$\text{SiH}_3^+$	Total
Energy (eV)							
12	-				0.85		0,85
13	-		-		6.70	2.34	9.04
14		-	0.20		22.8	10.4	35.2
15		-	0.69	0.49	44,4	26.2	71.8
16			0.98	0.89	71.7	47.6	121.2
17			1.47	1.67	99.2	63.9	166.2
18	-	-	2,16	2,95	119.8	80.6	205.5
19	-	-	2,75	5.21	139.5	93.8	241.3
20	-	-	3.73	9.5	151.3	101,7	266,2
22			6.39	19.45	169.0	110.0	304.8
24			10.5	32.6	180.7	113.9	337.7
26	0,73	0.098	15.7	44.2	187.9	116.1	364.7
28	2,06	0.786	22.3	51.1	190.9	117.2	384.3
30	5.80	1.57	29,0	56.0	191.8	117.9	402.1
32	6.88	2,16	33.4	57.9	190.6	117.9	408.8
34	9.43	2.75	37.3	58.3	189.4	117.2	414.4
36	12.2	3.19	40.3	58.0	188.1	116.9	418.7
38	14.7	3.24	41.7	57.5	186.4	116.7	420.2
40	17.5	3.54	43.4	58.2	<b>184.7</b>	<b>116.9</b>	424,2
45	22.2	3.54	45.2	58,9	180.9	118.9	429.6
50	25.9	3,21	45.4	57.3	176.9	120.1	428.8
55	27.7	2.95	44,7	54,0	174.7	120.9	425.0
60	28.5	2.82	43.2	5(L3	172.4	121.5	418,7

65	<b>28.6</b>	2.53	<b>41.9</b>	47.2	169.9	121,6	411.7
70	<b>28.5</b>	2.39	40.3	45.0	168.0	<b>121.5</b>	405.7
75	28.3	2.29	38.5	42.8	165.6	120.8	398.3
80	28.0	2.16	37.0	40.9	163.1	119.8	391.0
85	27.5	2.08	35.4	38.8	160.1	118.9	382,8
90	26.9	2.00	34.1	37.03	158.2	118.1	376.6
95	26.3	1.92	32.6	36.0	156.1	116.9	369.8
100	25.4	1.85	31.4	35.4	153,8	116.0	363.9
110	24.1	1.75	28.7	32.4	151.0	113.7	351.7
120	22.8	1.66	26.3	29.8	147.2	110.9	338.7
130	21.8	1.56	<b>24.4</b>	27.5	143.8	108.1	327.2
140	20.6	1.49	22.5	25.6	140.5	105,3	316.0
150	19.4	<b>1.41</b>	20.7	24.0	137.0	102.3	304,8
160	18,6	1.36	19.4	22.5	133.6	99.9	295.4
170	17.7	1.30	18.4	21.5	130.3	97.2	286.4
180	16,9	1.25	17.4	20.4	127.2	94.5	277.7
190	16.3	1.21	16.6	19.6	123.8	92.3	269.8
200	15.5	1.18	15.5	18.9	120.8	90,0	261.9
250	<b>13.1</b>	0.99	12,4	15.5	108.8	81.1	231.9
300	11.2	0,88	10.4	13.3	98,2	73.5	207.5
350	9.88	0.79	8.94	<b>11.7</b>	88.9	67.3	187.5
400	8.72	0.70	7.86	10,6	81.1	61,4	170.4
450	7.92	0.65	7.17	9,43	74.6	56.8	156.6
500	7,27	0,63	6,46	8.92	69.2	53.2	145.7
550	6.87	0,57	5.83	7.95	65.2	49.9	136.3
600	6.60	0,53	5.27	7.15	61.1	46.8	127.5
650	6.35	0.49	4.82	6,59	57.0	43.6	<b>118.9</b>

700	6.10	0.46	4.42	6.03	53.0	40.8	110.8
750	5.85	0,42	4.05	5,51	49.7	38.1	103.6
800	5.59	0.40	3.71	5,08	46.7	35.9	97.4
850	5,30	0.37	3.41	4.65	44.2	34.1	92.0
900	5.14	0.35	3.14	4,29	41.8	32.4	87.1
950	4.92	0.33	2.93	3.99	39,7	30.8	82.7
1000	4.73	0,31	2.73	3,71	38.0	29,2	<b>78.7</b>

TABLE 11, Appearance potentials (eV) of positive ions from SiH<sub>4</sub>

Ion	Present	Chatham <i>et al.</i> [8]	Morrison and Traeger [3]	Potzinger and Lampe [7]	Neuert and Clasen [4]
SiH <sub>4</sub> <sup>+</sup>	not observed	not observed	not observed	not observed	12,2
SiH <sub>3</sub> <sup>+</sup>	12.3±0.5	12.2	12.2	12.3	12,2
SiH <sub>2</sub> <sup>+</sup>	11.9±0.5	11.6	11.8	11.9	14.5
SiH <sup>+</sup>	14.7±0.5	15.01±1	14,7	15.3	14.5
Si <sup>+</sup>	13.6±0.5	13.5± 2	13,3	13.6	—
H <sub>2</sub> <sup>+</sup>	25.0±2	---	---	---	16,0
H <sup>+</sup>	24.5 ±2	---	---	---	22.4

TABLE 111. Partial and total ionization cross sections (10-18 cm<sup>2</sup>) of Si<sub>2</sub>H<sub>6</sub>

Electron energy (eV)	Si <sup>+</sup>	SiH <sup>+</sup>	SiH <sub>2</sub> <sup>+</sup>	SiH <sub>3</sub> <sup>+</sup>	Si <sub>2</sub> <sup>+</sup>	Si <sub>2</sub> H <sup>+</sup>	Si <sub>2</sub> H <sub>2</sub> <sup>+</sup>	Si <sub>2</sub> H <sub>3</sub> <sup>+</sup>	Si <sub>2</sub> H <sub>4</sub> <sup>+</sup>	Si <sub>2</sub> H <sub>5</sub> <sup>+</sup>	Si <sub>2</sub> H <sub>6</sub> <sup>+</sup>	Total
10	-	-	-	-	-	-	-	-	-	-	-	-
11	-	-	-	-	-	-	-	-	-	-	5.41	5.41
12	-	-	<b>0.0</b>	<b>0.0</b>	-	-	-	-	7.87	1.48	13.8	23.2
13	-	-	<b>1.18</b>	<b>1.18</b>	-	-	<b>2.95</b>	0.30	33.5	5.41	27.6	69.2
14	-	-	3.14	7.85	-	-	7.87	1.48	59.1	14.8	42.3	136.5
15	0.0	0.1	6.29	18.1	2.46	<b>0.0</b>	15.7	2.95	92.5	24.6	54.1	216.8
16	0.47	0.79	12.6	30.8	<b>7.58</b>	<b>0.69</b>	37.4	5.9	119.1	33.5	65.0	313.8
17	1.06	1.57	19.6	42.0	14.8	1.28	60.0	9.84	140.7	40.8	73.8	405.4
18	1.57	3.93	27.9	56.2	27.1	<b>2.95</b>	81.7	<b>15.7</b>	163.9	46.6	80.7	508.3
19	2.55	7.86	35.0	69.7	44.1	6.59	99.9	26.1	188.3	50.5	87.9	618.5
20	3.81	<b>11.8</b>	39.3	74.5	58.7	11.8	115.2	35.1	203.2	54.1	93.0	698.5
22	7.47	<b>25.5</b>	46.4	88.4	79.7	<b>35.9</b>	<b>146.7</b>	53.1	224.4	58.0	100.9	866.5
24	12.2	39.3	49.9	96.3	91.5	<b>65.9</b>	169.8	62.0	232.8	59.5	104.8	984.0
26	20.0	<b>55.0</b>	52.7	98.7	99.4	97.4	185.5	65.3	235.5	60.7	105.6	1075.8
28	26.3	<b>69.5</b>	54.1	99.9	100.6	122.0	195.9	65.6	236.0	61.2	105.3	1136.4
30	36.9	82.5	54.6	99.8	100.1	138.8	197.8	62.7	235.7	62.0	103.8	1174.7
32	49.1	<b>92.3</b>	54.7	98.8	97.4	150.1	196.4	59.5	234.5	62.9	102.4	1198.1
34	56.2	98.2	54.8	97.1	93.8	<b>153.3</b>	190.9	55.8	232.8	63.7	101.1	1197.7
36	62.9	100.6	54.7	94.9	89.6	150.4	184.7	53.1	230.1	63.8	99.9	1184.7
38	68.0	101.0	54.1	92.5	85.6	144.7	<b>179.7</b>	<b>50.4</b>	228.1	64.2	99.4	1167.1
40	70.3	102.9	53.0	89.6	81.9	135.8	171.2	48.2	225.2	64.8	100.2	1144.1
45	68.4	91.2	48.7	81.3	74.1	119.1	<b>159.4</b>	43.1	221.5	65.9	99.9	1072.6
50	61.3	81.7	44.8	74.1	69.6	108.8	<b>151.6</b>	40.4	220.8	67.1	100.6	1020.8
55	55.0	74.7	41.5	69.2	65.7	99.4	144.7	38.7	220.5	68.7	101.4	979.5

60	50.3	69.5	39.9	66.2	67.7	91.5	139.8	37.1	219.3	69.4	102.1	957.7
65	47.2	62,3	38.2	64.0	60.7	85.6	136.6	35.9	218.2	69.7	103.1	921.5
70	45.3	58.9	37.3	62.1	59.0	81,9	134.4	35,0	217.1	70.2	104.5	905.3
75	42.8	55.4	36.4	60,5	57.1	77.6	131.4	33.8	215.6	70.3	104.5	885.4
80	40.9	52.3	35.7	59,2	55.8	74.5	128.9	33.3	214.4	70.6	104.8	870.4
85	39.1	49.9	35.0	57.6	54.1	71.5	125.8	32.3	212.3	70.1	104.7	852.4
90	37.1	46.8	34,2	56.5	53.1	68.7	124.0	31.5	210.4	69.9	104.3	836.5
95	35.4	44.2	33.3	55.0	51.7	65.5	121.2	30.8	207.7	69.4	103.3	817.5
100	33.8	42.2	32.6	54.0	50.4	63,0	119.1	30,3	205.7	68.9	102.3	802.3
110	31.0	38.7	31.4	51.5	48.0	59,0	115.2	28.5	200.3	67.4	100.2	771.2
120	28.9	35,8	30.1	49.7	46.0	54.1	109.7	27.3	194.9	65.9	97.9	740,3
130	26.7	33,0	28.7	47.4	43.9	50.2	105.3	2,6,4	189,0	64.7	95.5	711.2
140	25.0	31.0	27.5	45.9	42,1	46.6	101,2	25.3	183.9	63	93.5	685.0
150	23.3	29.1	26.5	44.5	40.8	43.5	97.9	24,4	179.1	61.8	91.0	661.9
160	22.0	27,5	25,7	42.9	38.9	40.6	94.3	23.3	174,2	60.0	88,6	638.0
170	20.4	25.9	24.8	41,7	37.3	37.9	90.8	22,4	170.5	58.2	86.6	616.5
180	19.3	24.8	24.0	40.3	36.4	35.6	88.4	21.8	166.0	57.1	84.6	598,3
190	18.3	23.8	23.2	39.1	35,1	34.1	85,6	20,9	161.4	55.9	82,7	580.1
200	17.3	22,4	22.2	38.0	34.3	32.5	83.7	2,0,4	158,5	54.7	81.5	565.5
250	13.4	18,1	19,1	32.6	29.3	26.4	73,6	17.9	142.7	49.2	73.0	495.3
300	10.9	14.9	16.8	28.7	25.6	21.6	65,0	15,6	129.9	45.1	65.7	439.8
350	9.0	12.6	14.5	25.8	23.4	18.6	58.6	14,5	119.8	42.2	60,0	399.0
400	7.91	10.8	13.2	23.1	21.2	15.9	53.8	13.1	111.2	39.4	54.9	364.5
450	6.88	9,43	12,1	21.1	19.4	11.9	48.9	11,7	104.0	36.4	50.3	332.1
500	6.29	8.64	11.0	19.4	17.7	12.6	45.1	10.6	97.2	34,1	46.9	309.5
550	5.62	7.74	9.96	18.0	16,0	11.4	42.7	9.96	92.7	32.5	44.2	290.8
600	5,13	7.05	9.27	16.6	14.3	10.5	40.1	9.33	88.6	31.1	42.1	274.1

650	4,64	6.39	8.66	15,5	13,0	9.54	37.5	<b>8.76</b>	84.6	29.8	40.6	258.0
700	4.24	5.84	8.12	14,4	12.0	<b>8.83</b>	35.5	8.29	80.9	28.6	38.6	245.3
750	3.89	5.36	7.62	13.5	11,0	8.21	33.9	7.85	77,9	27.1	36.9	233.5
800	3.59	4.95	7.13	12.7	10.2	7.64	32.3	<b>7.45</b>	75,0	26,2	35.5	222.7
850	3.33	4.59	6.72	<b>11.9</b>	9.48	7.14	30,6	<b>7.06</b>	71.9	25.2	34.1	212.0
900	3.09	4,25	6.31	11,3	8.84	6,70	29.3	6.71	69.0	24,3	32.9	202.7
950	2.87	3,97	5.95	<b>10.7</b>	8.27	<b>6.31</b>	27.7	<b>6.36</b>	66.5	23.5	31.8	<b>193.9</b>
<b>1000</b>	<b>2.71</b>	3.73	5.64	10.2	7.77	5.97	26.4	<b>6.12</b>	64.4	22.8	30.9	186.6

TABLE IV. Appearance potentials (eV) of positive ions from  $\text{Si}_2\text{H}_6$

Ion	Present	Chatham <i>et al.</i> [8]	Potzinger and Lampe [7]
$\text{Si}_2\text{H}_6^+$	$10.2 \pm 0.5$	9.9	10.15
$\text{Si}_2\text{H}_5^+$	$11.7 \pm 0.5$	11.2	11.4
$\text{Si}_2\text{H}_4^+$	$11.0 \pm 0.5$	10.8	10,85
$\text{Si}_2\text{H}_3^+$	$12.8 \pm 0.5$	$12.0 \pm 1$	12.5
$\text{Si}_2\text{H}_2^+$	$12.2 \pm 0.5$	11.5	11.8
$\text{Si}_2\text{H}^+$	$15.0 \pm 1$	$15 \pm 2$	12.9
$\text{Si}_2^+$	$14.5 \pm 1$	$17.5 \pm 3$	13.0
$\text{SiH}_3^+$	$12.0 \pm 0.5$	$11.0 \pm 2$	11.95
$\text{SiH}_2^+$	$12.0 \pm 0.5$	$10.0 \pm 2$	11.95
$\text{SiH}^+$	$14.7^* 0.5$	$14.0 \pm 2$	
$\text{Si}^+$	$15.0 \pm 0.5$	$15 \pm 2$	

TABLE V. Coefficients obtained by fitting the partial ionization cross sections for  $\text{SiH}_4$  to the parametrised form as given in Eq. 1. The appearance potentials have been taken from our measured values given in Table II.

Jon	A	$a_1$	$a_2$	$a_3$	$a_4$	$a_5$	$a_6$
H <sup>+</sup>	383.928	-273.800	-462.094	4207.379	-2766.207	—	.
H <sub>2</sub> <sup>+</sup>	22,75	-18.462	432.258	75,791	-32.54.724	4921.341	-2161,974
Si <sup>+</sup>	24.865	-106.416	1992.041	-12785.320	32427.344	-30812,676	9582,563
SiH <sup>+</sup>	33.505	299,796	-5228.592	26444.697	-46162,402	35138.918	-10001,181
SiH <sub>2</sub> <sup>+</sup>	1132.677	-1026,057	-1638.357	18130.305	-36137.832	20716,961	—
SiH <sub>3</sub> <sup>+</sup>	899,380	-922.381	-359.580	15613.208	-46354.133	46379,555	-14372.854
Total ion	2143.024	-2327,962	1702,468	10220,521	-25086,850	16272,706	—

TABLE VI. Coefficients obtained by fitting the partial ionization cross sections for  $\text{Si}_2\text{H}_6$  to the parametrised form as given in Eq. 1. The appearance potentials have been taken from our measured values given in Table IV.

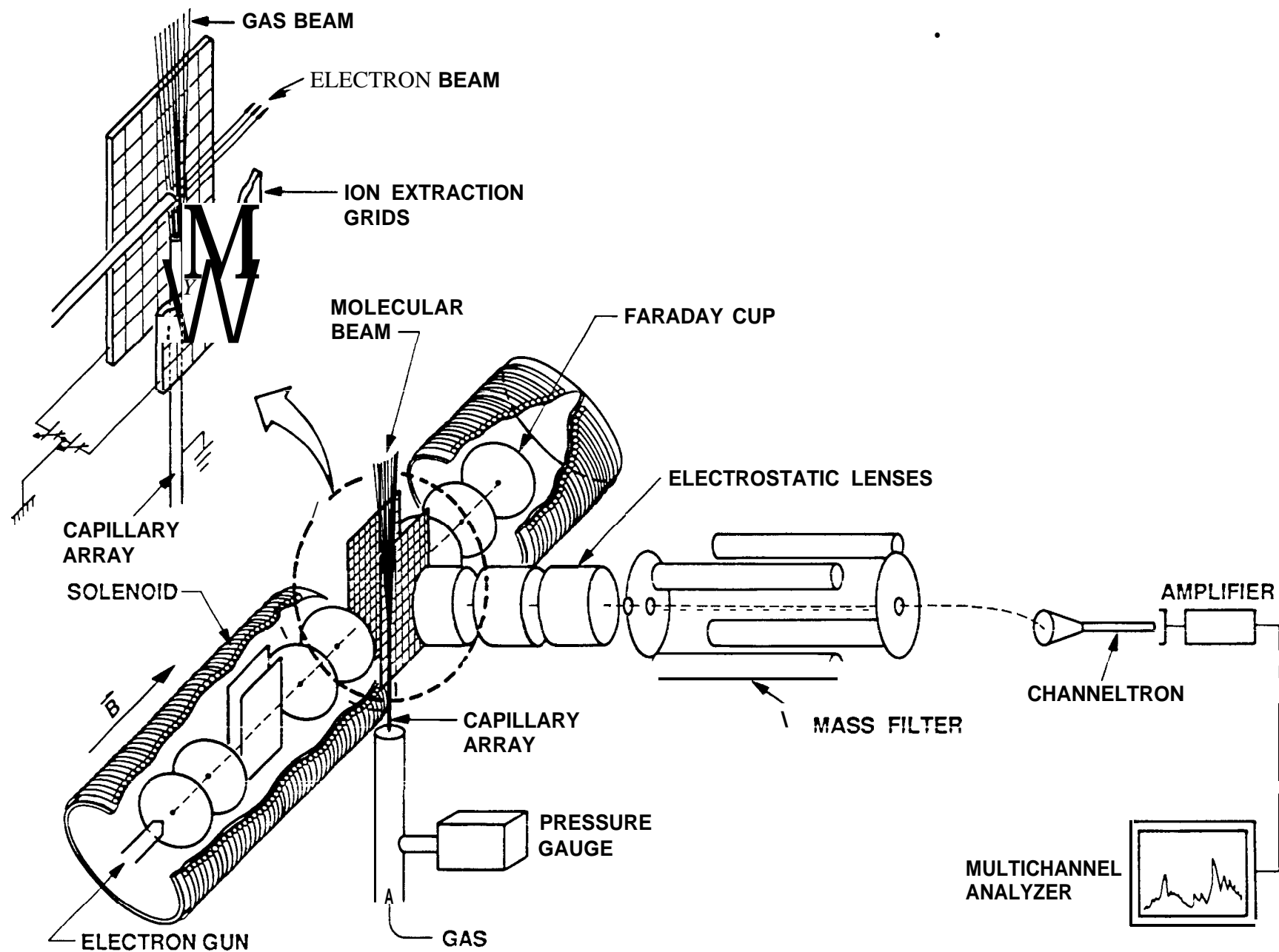
Ion	A	$a_1$	$a_2$	$a_3$	$a_4$	$a_5$	$a_6$
$\text{Si}^+$	-439.553	257.591	5955.866	-44142.066	133819.750	-160558.562	67082.141
$\text{SiH}^+$	-646.234	675.941	2414.333	-25398.727	106093.273	-150114.797	69826.555
$\text{SiH}_2^+$	5.480	16.640	-335.776	2981.240	459.067	-9219.888	6851.284
$\text{SiH}_3^+$	-15.949	-90.301	1830.298	-5610.815	24180.061	-40830.699	21982.279
$\text{Si}_2^+$	-316.221	264.364	1312.396	112.41.229	-2.9120.379	19014.088	—
$\text{Si}_2\text{H}^+$	-918.234	2336.170	-20333.596	922.24.367	-134394.0	65048.125	—
$\text{Si}_2\text{H}_2^+$	52.852	-55.133	1149.670	-8254.867	572.51.281	-101481.914	54544.945
$\text{Si}_2\text{H}_3^+$	-72.239	583.160	-7899.672	39976.320	-72381.695	52914.258	-12076.016
$\text{Si}_2\text{H}_4^+$	2058.287	-1792.120	-3501.287	21299.633	-38694.426	20272.900	—
$\text{Si}_2\text{H}_5^+$	782.647	-831.074	1033.076	-1271.496	-2219.039	2369.074	—
$\text{Si}_2\text{H}_6^+$	827.488	-582.16	-2905.371	13'733.095	-2.3416.209	12486.139	—
Total ion	5281.283	-5640.265	12001.550	-117384.664	390366.531	-483075.594	199514.531

## FIGURES

FIG. 1. Schematic diagram of the experimental arrangement

FIG. 2. Partial ionisation cross sections for **silane**: The hollow symbols and the stars represent the present data and the filled symbols and the crosses represent the data from [8] with circles for  $\text{SiH}_3^+$ , inverted triangles for  $\text{SiH}_2^+$ , squares for  $\text{SiH}^+$ , triangles for  $\text{Si}^+$ , diamonds for  $\text{H}_2^+$ , and the stars and crosses for  $\text{H}^+$ . The  $\text{H}_2^+$  and  $\text{H}^+$  data have been multiplied by a factor of five for clarity of presentation.

FIG. 3. Partial ionisation cross sections for **disilane**: (a) The hollow symbols are for the present data and the filled symbols are for the data from [8] with circles for  $\text{Si}^+$ , inverted triangles for  $\text{SiH}^+$ , squares for  $\text{SiH}_2^+$ , triangles for  $\text{SiH}_3^+$ , and diamonds for  $\text{Si}_2^+$ . (b) The hollow symbols and stars are for the present data and the filled symbols and crosses are for the data from [8] with circles for  $\text{Si}_2\text{H}^+$ , inverted triangles for  $\text{Si}_2\text{H}_2^+$ , squares for  $\text{Si}_2\text{H}_3^+$ , triangles for  $\text{Si}_2\text{H}_4^+$ , diamonds for  $\text{Si}_2\text{H}_5^+$ , and the stars and crosses for  $\text{Si}_2\text{H}_6^+$ .



**SCHEMATIC DIAGRAM OF THE EXPERIMENTAL ARRANGEMENT**

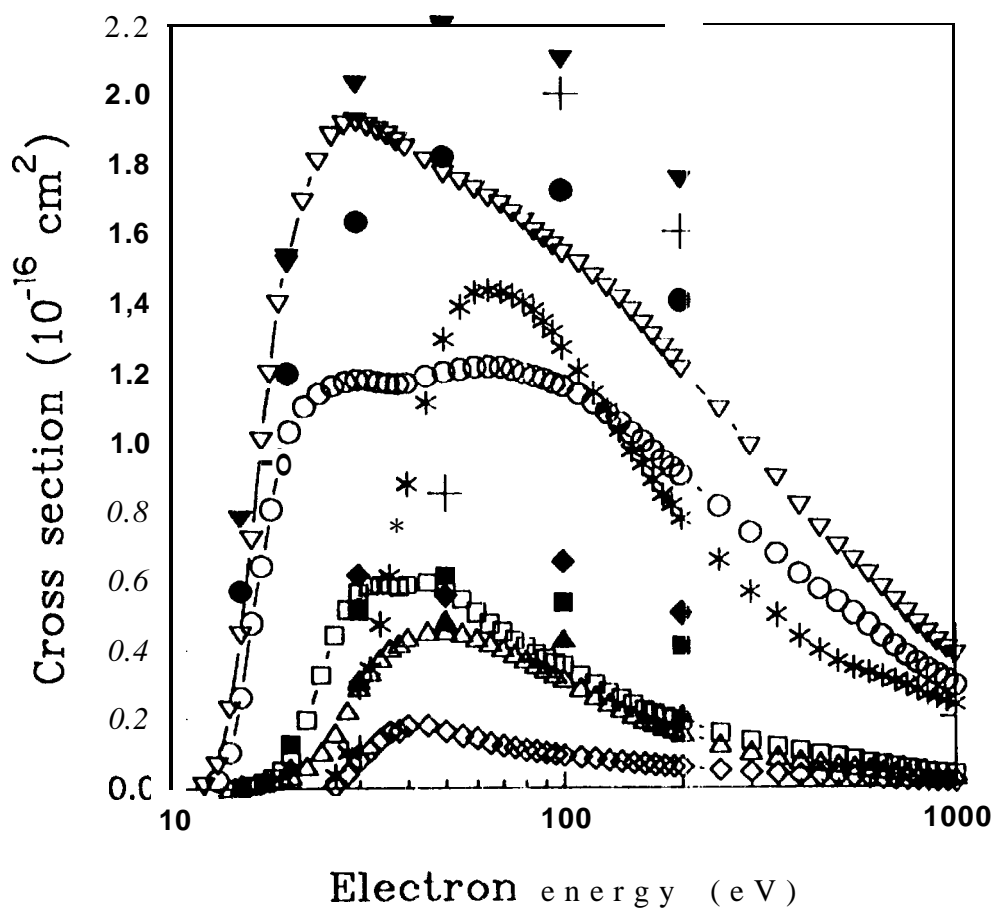


Fig 2 Krishnakumar and Oriskalo

